Send Orders for Reprints to reprints@benthamscience.ae

The Open Fuels & Energy Science Journal, **2015,** *8,* **1-13**

Open Access

Numerical Investigation on the Flow, Combustion and NO_x Emission Characteristics in a 10 MW Premixed Gas Burner

Weibo Chen and Guixiong Liu*

School of Mechanical & Automotive Engineering, South China University of Technology, Guangzhou, China

Abstract: The characteristics of the combustion temperature, flow velocity, CO distribution and NO_x emissions of a 10 MW gas burner at different primary to secondary air ratios are numerically studied using computational fluid dynamics software Fluent. The results indicate that the primary to secondary air ratio in gas burner determines the combustion quality through influencing some parameters directly, such as the combustion efficiency, combustion intensity, profile and stability of flame as well as emission of NO_x. Then two evaluation indexes of combustion quality are summarized after analyzing the flame structure and characteristics of the flow. The detailed results reported in this paper may provide a useful basis for NO_x reduction and premixed gas burner design. Finally some proposals are given to choose the optimal primary to secondary air ratio for a gas burner.

Keywords: Combustion, computational fluid dynamics, energy, numerical simulation..

1. INTRODUCTION

Gas burners are a kind of device which jet the flaming gas mixed with fuel gas and air. They are used necessarily in heating energy and related industries, for example, boilers, smelting furnaces and thermal treatment. It controls thermal load, temperature distribution, thermal efficiency and working life of the controlled object because it's the core of the whole heating equipment [1-8]. Some experimental results indicate that expansive shape of fuel is significantly influenced by the structures and dimensional parameters of fuel injection systems [2]. Fuel jet velocity and air velocity affect the blow-off behavior of Swirl-Stabilized Premixed, Non-Premixed and Spray Flames [5]. When the burners are working, combustion efficiency and intensity of fuel and stability of flame have decisive influences on combustion quality. And these parameters above depend on the supply situation of oxygen in the combustion process [9-12]. The unsatisfactory situation of oxygen supply may be due to lack of air or inappropriate proportion of primary air which mixed with fuel gas and secondary air participating in combustion. So in a certain amount of total air, the primary to secondary air ratio has a remarkable influence on the flame temperature, flow velocity distribution and NO_x emission. Technology of computational fluid dynamics (CFD) is wildly used in the research field of thermal energy such as combustion studying [9, 13-15]. Different kinds of models and methods are utilized to simulate all kinds of characteristics of flames [1, 7, 15]. It is necessary to simulate the combustion characteristics of the gas burner since CFD technology can provide more details of the flow field than experiment.

*Address correspondence to this author at the School of Mechanical & Automotive Engineering, South China University of Technology, Guangzhou, China; Tel: +86-20-87110568; Fax: +86-20-87110568;
E-mail: megxliu@scut.edu.cn

In this paper, a kind of premixed gas burner produced was taken for instance. Combustion situations inside a boiler furnace at different primary to secondary air ratios were simulated using CFD software Fluent. The characteristics of temperature, flow velocity, NO_x distribution and flame profiles have been analyzed to study how the primary to secondary air ratio affects the combustion quality. The results have important significance for both combustion quality and burner structure improvement.

2. NUMERICAL ANALYSIS PROCEDURE

2.1. Flow Fields of Burner

The structure of premixed gas burner is shown schematically in Fig. (**1a**). Its air-inlet is a rectangle which has a width of 0.400 m and a length of 0.711 m. The nozzle of burner is a circle with a diameter of 0.340 m. In order to reduce computational domain for computation, air flow field inside the whole burner has been simulated by CFD software before the combustion simulation. Then appropriate primary to secondary air ratios as well as air velocity would be chosen as boundary conditions for combustion numerical simulation according to the simulation results of the air flow field. Calculation models of three opening degrees (15°, 30°, 45°) of the secondary air door are built for numerical simulation according to the structure of the gas burner. The value of coefficient of excess air is 1.08. The volume flow rate of air actually needed is 2.8866 m^3/s when the gas burner is working nearby the rated thermal load.

Fig. (**1b-d**) shows the situations of the air velocity distribution with different opening degrees of the secondary air door. The air speed inside the air door decreases as the opening degree of the secondary air door increases. And there are some distinctions of velocity distribution. When the opening degree is 15°, air velocity nearby the secondary air door is the highest and it decreases down along the outlet

1876-973X/15 2015 Bentham Open

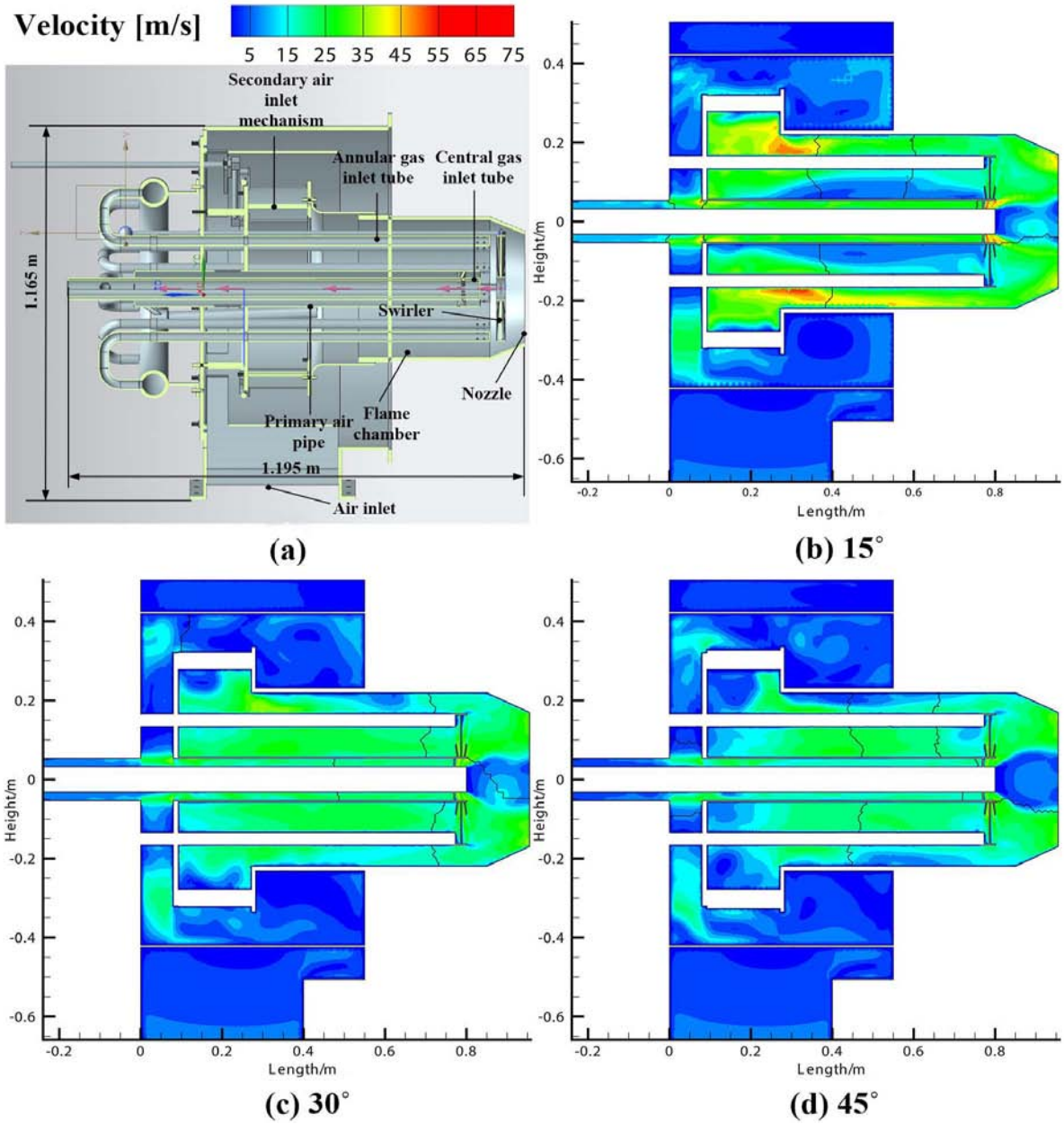

Fig. (1). Structure of the premixed gas burner (**a**) and velocity distributions of airflow with different opening degrees of the secondary air door (**b**) (**c**) (**d**).

down to a minimum velocity of about 9.18 m/s near the primary air pipe in the lower area of secondary air door. The highest speed (78.10 m/s) appears nearby the secondary air door. When the opening degree is 30°, the total velocity distribution is not the same as the situation of 15°. Air speed near air door is relatively low. It increases first and falls a bit toward the outlet. The maximum value of velocity appearing in the upper area of the combustion chamber is about 54.20 m/s. It increases obviously after passing through the swirler. When the opening degree is 45°, the total velocity distribution is similar to the situation of 30°, but the average velocity is lower. The highest speed appears in the area near the secondary air door. After passing through the swirler, the air velocity increases slowly and achieves to top speed of 38.50 m/s. A swirling flow formed *via* the air flow passing the swirler is found in the middle of the area between the swirler and the nozzle. It continuously absorbs flue gas from the outlet. The velocity distribution of air when it enters into combustion chamber is relatively uniform. Result details show that only primary to secondary air ratios and the swirler has remarkable influences on the situations of the airflow ejected from the burner. This phenomenon should be considered to simplify the computational domain in combustion simulation. The primary to secondary air ratios under conditions of different opening degrees of secondary air door can be obtained by calculating the mass flow of air passing into the primary pipe and secondary air inlet mechanism respectively.

2.2. Model Building and Meshing

Since gas burner is a key component of the combustion system, its most direct effect is to heat the boiler furnace. When the burner is working, flame is spraying out from the combustion chamber into the boiler furnace, so most of the flames, high temperature flue gas and NO_x pollutants are generated in the furnace. Establishing burner-combustion chamber model to simulate the normal operation of the burner can make the computed result more close to the real situation. The thermal load of premixed gas burner used throughout this paper is 10 MW. The shape and size of the furnace model were determined based on the 12 t/h boiler equipment. In order to facilitate the study of the impact of the primary air, secondary air and the fuel flow to the combustion quality, considering the velocity distribution of air inside the burner obtained by simulation in the previous section simultaneously, the simulation model shown in Fig. (**2a**) only contains the combustion chamber of burner and boiler furnace. Fig. (**2b**) exhibits the magnification of combustion chamber of the simplified model. And representative primary to secondary air ratios were determined by the characteristics of the air flow field simulated. SolidWorks 2012 and ICEM software were used to build the model and create triangular unstructured grids respectively. Moreover, the body-fitted meshing technique was employed. In the combustion chamber of the burner and region near the burner jet, finer grids were generated, while in regions far away from the flame base and the axis coarser ones were generated. In this way, a primary mesh with a total of 9,118,314 tetrahedral cells was generated (shown in Fig. **2c**).

After the grid-independency of the results was verified using a finer mesh with 18,118,314 cells, which had been indicated by the fact that the results (including the flow structure, velocity distribution, temperature iso-contours of 2000 K) for the case of primary to secondary air ratio 7.925% using the two different meshes were kept in high consistency (shown in Fig. **3**), the primary mesh was finally employed for solving all other cases.

2.3. Computational Models

The combustion simulations were carried out using the commercial CFD package ANASYS FLUENT. Numerical calculations of the present problem included solutions of the Favre-averaged form of mass, momentum, energy, species, turbulent kinetic energy k, and its dissipation rate ε transport equations available in FLUENT.

In addition, the realizable k−ε model with the standard wall function was employed to predict the turbulence in the combustion system. In this paper, the non-premixed model was used for combustion, a mixture-fraction equation is solved instead of equations for individual species, and the individual species concentration is derived from the predicted mixture fraction concentration under the assumption of chemical equilibrium. Interaction between turbulence and chemistry is accounted for with the β-function probability density function (PDF). The SIMPLE algorithm was used to solve the pressure-velocity coupling, and a second-order discretization scheme was utilized to solve all governing equations.

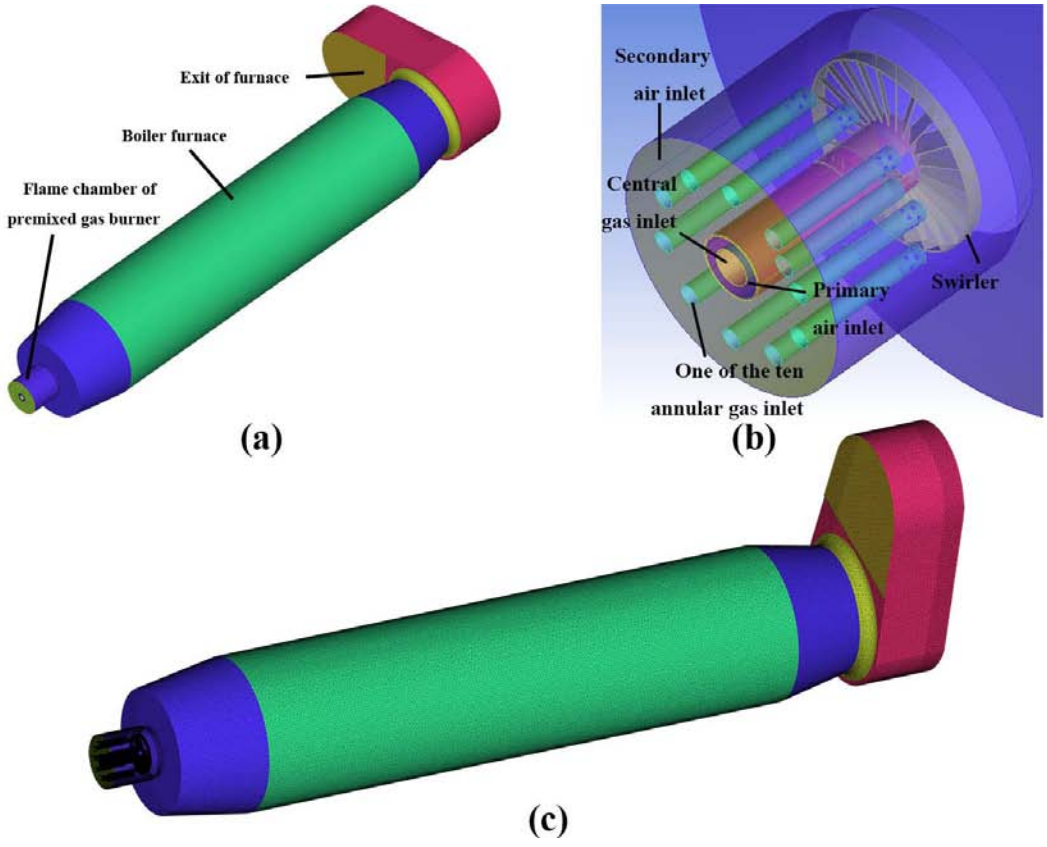

Fig. (2). Schematic of the burner-combustion chamber model (**a**) (**b**) and mesh system of the model (**c**).

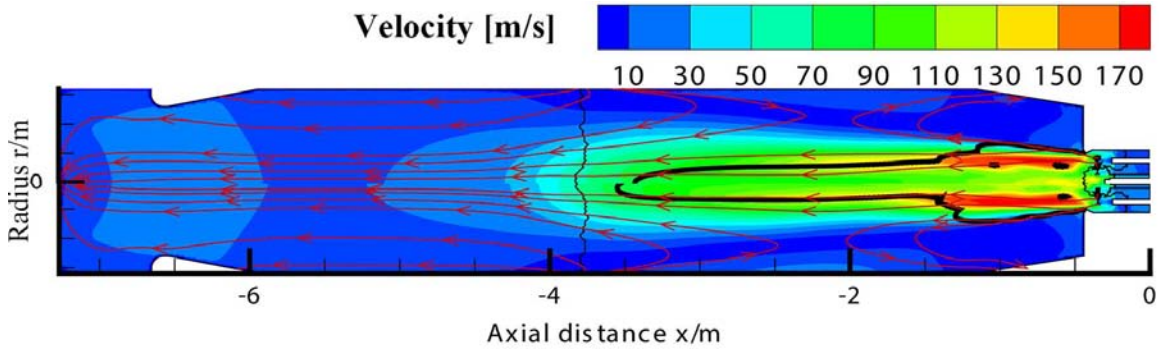

Fig. (3). Verification of grid-independency for case of primary to secondary air ratio 7.925%. (The upper is for the coarse grids with 9,118,314 cells and the lower is for the fine grids with 18,118,314 cells. The velocity distribution is shown in rainbow color. The streamlines, temperature isocontours of 2000 K (the black solid line) are superimposed on it).

2.4. CH_4-Oxidation and NO_x-Formation Modeling

CH_4 combustion reactions are highly complex, and are normally simplified into a series of global reactions with CFD modeling. A typical reactions scheme can be summarized in the form [16]:

$$CH_4 + \frac{1}{2}O_2 \rightarrow CO + 2H_2 \quad (1)$$

$$CO + \frac{1}{2}O_2 \rightarrow CO_2 \quad (2)$$

$$H_2 + \frac{1}{2}O_2 \rightarrow H_2O \quad (3)$$

After the combustion calculation, the NO_x calculation is performed based on the predicted temperature and species concentrations under the assumption that the NO_x concentration is very low and, therefore, has a negligible impact on the natural gas combustion. NO_x is formed mainly by thermal NO_x formation mechanisms. A transport equation for the NO species (i.e., NO, NO_2, N_2O) is calculated, which takes into consideration convection, diffusion, production and consumption of NO species.

$$O + N_2 \underset{k_r,1}{\overset{k_f,1}{\rightleftarrows}} N + NO \quad (4)$$

$$N + O_2 \underset{k_r,2}{\overset{k_f,2}{\rightleftarrows}} O + NO \quad (5)$$

$$N + OH \underset{k_r,3}{\overset{k_f,3}{\rightleftarrows}} H + NO \quad (6)$$

where

k_f = forward reaction rates.

k_r = reverse reaction rates.

The value of k_f and k_r are determined based on the evaluation of Hanson and Salimian [9].

For the above thermal NO_x mechanisms, only a NO species transport equation is required:

$$\frac{\partial}{\partial t}\left(\rho Y_{NO}\right) + \nabla \cdot \left(\rho \vec{v} Y_{NO}\right) = \nabla \cdot \left(\rho D \nabla Y_{NO}\right) + S_{NO} \quad (7)$$

Table 1. Analysis data of the liquefied natural gas used for simulation.

Parameter		Value
species	CO_2 (*w*%)	0.5
	CO (*w*%)	0.1
	CH_4 (*w*%)	95
	H_2 (*w*%)	1
	N_2 (*w*%)	1
	O_2 (*w*%)	0
	C_mH_n (*w*%)	2.4
	H_2S (mg/m^3)	400
	H_2S (mg/m^3)	100
	H_2O (mg/m^3)	0.2-2
lower calorific value	Q_{ar}^{dw}	35588 H_2S (kJ/m^3)/8850(H_2S (kcal/m^3))
standard density	ρ(kg/m^3)	0.718

where

Y_{NO}= mass fraction of NO species in the gas phase

D=effective diffusion coefficient

S_{NO}=source term for NO species.

The net rate of formation of NO species *via* Eqs. (4)-(6) is given by

$$\frac{d[NO]}{dt} = k_{f,1}[O][N_2] + k_{f,2}[N][O_2] + k_{f,3}[N][OH] - k_{r,1}[NO][N] - k_{r,2}[NO][O] - k_{r,3}[NO][H] \quad (8)$$

where all concentrations have units of gmol/m^3. The concentrations of O, H, and OH are calculated by the partial equilibrium approach [17].

2.5. Calculation Conditions Setting

According to the situations of flow field under the conditions of three different secondary air door opening degrees obtained by the previous numerical simulation, in order to better analyze the impact of different primary to secondary air ratios to combustion quality, the proportions selected to research are 15.000%, 7.925% and 5.985%, and the coefficient of excess air is 1.08. The fuel used in the simulation is liquefied natural gas (LNG) and the parameters of LNG used are shown in Table **1**.

The first step in setting the boundary conditions is calculating the actual amount of air to reach the thermal load of 10 MW of burner according to the formulas (9)-(10). The fuel consumption rate of 0.2838 m^3/s has been calculated when the burner was designed, and the coefficient of excess air α is defined as 1.08.

Theoretical amount of air required for the gas combustion is calculated as follows:

$$V^0 = 0.264\frac{Q_{ar}^{dw}}{1000} + 0.02 \tag{9}$$

where Q_{ar}^{dw} represents the lower calorific value of natural gas. Actual amount of air required for the gas combustion is calculated as follows:

$$V = \alpha V^0 \tag{10}$$

where α is the coefficient of excess air. The actual amount of air required unit time is determined as follows:

$$V_k^0 = V_r \cdot V \tag{11}$$

where V_r is the volume of fuel consumed.

Setting the boundary conditions need to calculate velocities, turbulence intensities and hydraulic diameters of the primary air pipe and secondary air mechanism outlet, central gas tube outlet and annular gas tube exit. The three volumes are calculated according to Eqs. (12)-(14). And all desired boundary conditions are obtained through considering formulas (9)-(10) simultaneously.

The results are shown in Table **2**. The parameters in the table are used as boundary conditions of the simulation. The hydraulic diameters of one single annular gas pipe outlet and central gas tube outlet are 6 mm and 5 mm respectively. There are total 80 annular gas pipe outlets at the end of the annular gas pipe and 12 central gas tube outlets at the end of the central gas tube in the burner.

The calculation formulas of velocity, turbulence intensity and hydraulic diameter are determined as Eqs. (11), (12), and (13) respectively:

$$v_0 = \frac{V_0}{A} \tag{12}$$

$$D_H = 4 \times \frac{S}{P} \tag{13}$$

$$I = 0.16 \times \left(\frac{v_0 D_H}{\nu}\right)^{-1/8} \tag{14}$$

where

V_0 = volume flow rate of gas needed (m^3/s)

A = sectional area of outlet (m^3)

S = infiltration cross-sectional area of pipe (m^3)

P = perimeter of infiltration cross-sectional area of pipe (m)

ν = kinematic viscosity of gas (m^2/s)

After setting boundary conditions in accordance with three different proportions of primary air in the total amount of air 5.985%, 7.925% and 15.000% respectively, the FLUENT solver was started to simulate.

3. RESULTS AND DISCUSSION

3.1. Validation of the Numerical Results

To validate the simulation results, the predicted velocity and species profiles were compared with the measured data. Fig. (**4**) shows the radial profiles for the velocity and O_2 mass fractions at line A-B which is 10 cm apart from the burner nozzle at the center cross-section of the furnace (shown in Fig. **5b**).

Results of the error analysis indicated that the average relative errors for the predicted velocities and O_2 mass

Table 2. Boundary conditions for combustion simulation.

Boundary Conditions	Proportion of Primary Air (%)	Outlet of Primary Air	Outlet of Secondary Air	Outlet of Annular Gas Pipe	Outlet of Central Gas Tube
Airflow velocity (*m*/*s*)	5.985	29.08	20.05	115.47	66.54
	7.925	38.5	19.63		
	15.000	72.87	18.12		
Turbulence intensity (%)	5.985	4.38	3.44	4.14	4.54
	7.925	4.19	3.45		
	15.000	3.85	3.49		
Hydraulic diameter (*mm*)	5.985	32.00	196.80	6.00	5.00
	7.925				
	15.000				

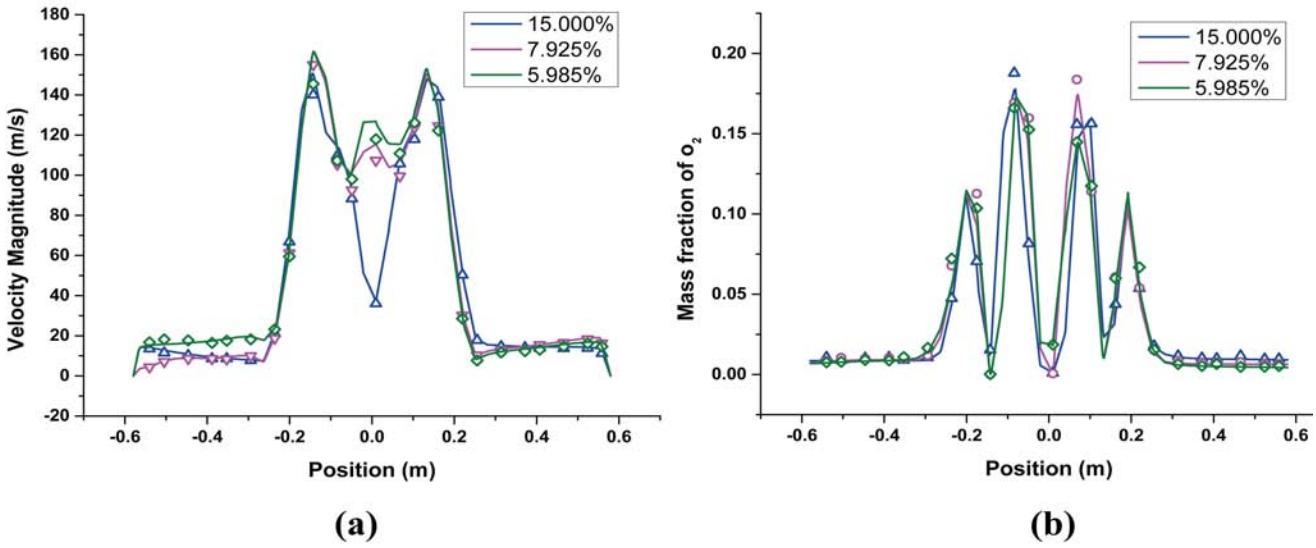

Fig. (4). Comparison of the measured and calculated velocity (**a**), O_2 mass fraction (**b**) distributions along the line A-B (Lines represent the predicted results and scattered symbols represent the measured data).

fractions were kept within ± 4.3% and ±1.9% respectively. The predictions agreed well with the measurements. This means that the adopted numerical models in the present calculations are reasonable for combustion analysis and NO_x emissions in the boiler**.**

3.2. Velocity Distributions

Velocity distributions inside the boiler furnace under conditions of different primary to secondary air ratios are shown in Fig. (**5**). There are some similarities of the flow field inside the furnace. A swirling flow is found between the inner and outer layers of flames. This area has the highest velocity of above 172 m/s and the temperature of 2000 K above. The O_2 concentration here is almost zero. This is explained by the fact that the gas here is high-temperature flue gas sucked back in front of the flames. It can ignite the fresh mixture air to stabilize flames.

Meanwhile, there is also a swirling flow inside the inner flames, but its speed of about 120 m/s and temperature of about 1500 ~ 1700 K are relatively low.

Rules of how primary to secondary air ratio affects flame shapes are summarized through comparing Fig. (**5c**) which show velocity profiles under conditions of different primary to secondary air ratios. In the range under blow-off limit, as the quantity of primary air increases, both the maximum speed and overall speed of flames increases. The velocity and swirl strength of the inner flames is also increasing. The peripheral contour of flames is shrinking and the heating zone becomes more concentrated while the capacity of swirling flow to suck high temperature flue gas is enhancing. So flame stability is improved. Characteristics of velocity are similar to the flame temperature distributions analyzed in section 3.3. When the proportion of primary air is 15.000%, flame combustion efficiency, stability and intensity of flames are optimum among the three proportions.

A conclusion is proposed that the effect of the combustion is the best when the proportion is 15.000% and the worst when the proportion is 5.985%.

Variations of velocity of line A-B is shown in Fig. (**4a**). When the proportion of primary air is 5.985%, the velocity in the central area is the slowest, however, the strength of the swirling flow is insufficient and the capacity to suck the high temperature flue gas is poor. So the combustion here is the most complete and it creates a maximum of flue gas. This makes the fastest speed in the central region among three proportions. Since the amount of secondary air outside the flames is the highest, the total speed in line A-B is the fastest when the proportion of primary air is 5.985%.

3.3. Temperature Distributions

Fig. (**6**) shows the temperature distributions in the horizontal cross section of the boiler furnace. The flames profile can be demonstrated by analyzing simulation results. The flames are divided into inner and outer flames both have doughnut-shapes. The outer flames are formed by the fixed gas sprayed from swirler. This part of gas consists of the liquefied natural gas jetted from the nozzle of the annular gas pipeline and the secondary air. Since there is a small amount of fuel but excessive oxygen in the outer flames, the combustion reaction was complete so quickly. The outer flames have a shorter length which only about half of the inner flames. And their temperature is lower. The inner flames are formed by fixed gas which consists of small amounts of gas ejected from the annular gas pipeline and sucked by the swirling flow in front of the combustion chamber outlet and gas ejected from the central gas tube and primary air. This part of the flames has a longer combustion process and flame length and higher temperature due to the sufficient fuel. It could be regarded as the main flame heating the furnace. Fig. (**6**) also shows the temperature is lower in the central portion of the flames. Because the center of the flame contains excess fuel, the oxygen content is

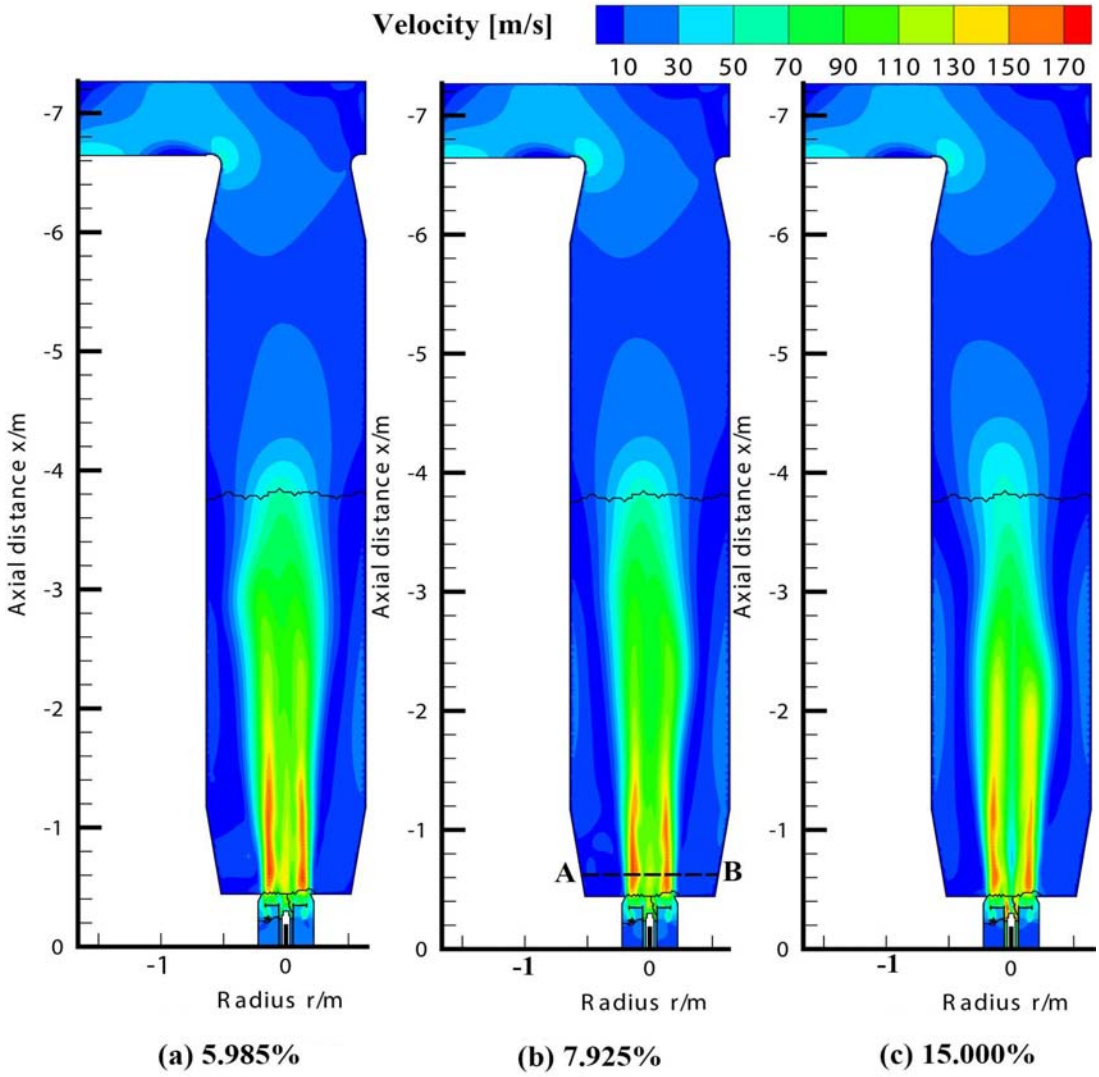

Fig. (5). Velocity distributions at different primary to secondary air ratios.

relatively lower. There is almost no combustion reaction occurring in this area. The more outward from the centre, the O_2 concentration relatively increase and the combustion reaction becomes more drastic. The temperature rises up until the O_2 concentration is zero. The temperature reaches the highest value when the reaction is stopped. Outside the flames, temperature of furnace maintained the maximum value of about 2240 K until a sharp decrease appears in the exit of the furnace.

In addition to the common characters of gas burning flame analyzed above, rules of how primary to secondary air ratio affects flame temperature distributions are summarized through comparing Fig. (**5a-c**) which show velocity profiles under conditions of different primary to secondary air ratios. As the proportion of primary air increases, the amount of air mixed with the gas out of center gas pipe becomes larger and combustion reaction of the inner flames is accelerated. The length of flames becomes shorter and the region which has a lower temperature inside the furnace gradually becomes lathy, indicating that the flames focus and better heat the furnace.

Variations of temperature of line A-B which is 10 cm apart from the combustion chamber outlet at the center cross-section of the furnace is shown in Fig. (**7a**). When the proportion of primary is 15.000%, oxygen content in the center of the flame is higher than that of proportions of 7.925% and 5.985%, so it has the fastest combustion efficiency and the highest temperature among three of them. When the proportion of primary is 5.985%, the oxygen content is less than that of 7.925%, but the slower velocity makes more time for mixing oxygen and gas in this region, so combustion reaction is faster. Temperature outside the flames is much higher than that of the flame center. From the figure, sizes of the flame structure are obtained. Shape of inner flames presents a circle with an inner radius of 0.02 m and an external radius of 0.14 m. Center of this circle is at the middle of the combustion chamber outlet. The shape of the outer flames which has an inner radius of about 0.14 m and an outer radius of 0.28 m is similar to that of the inner flames. Maximum value of flame temperature is 2230 K.

Through analyzing the temperature distributions in this line and the results of flame shapes analyzed in section 3.2,

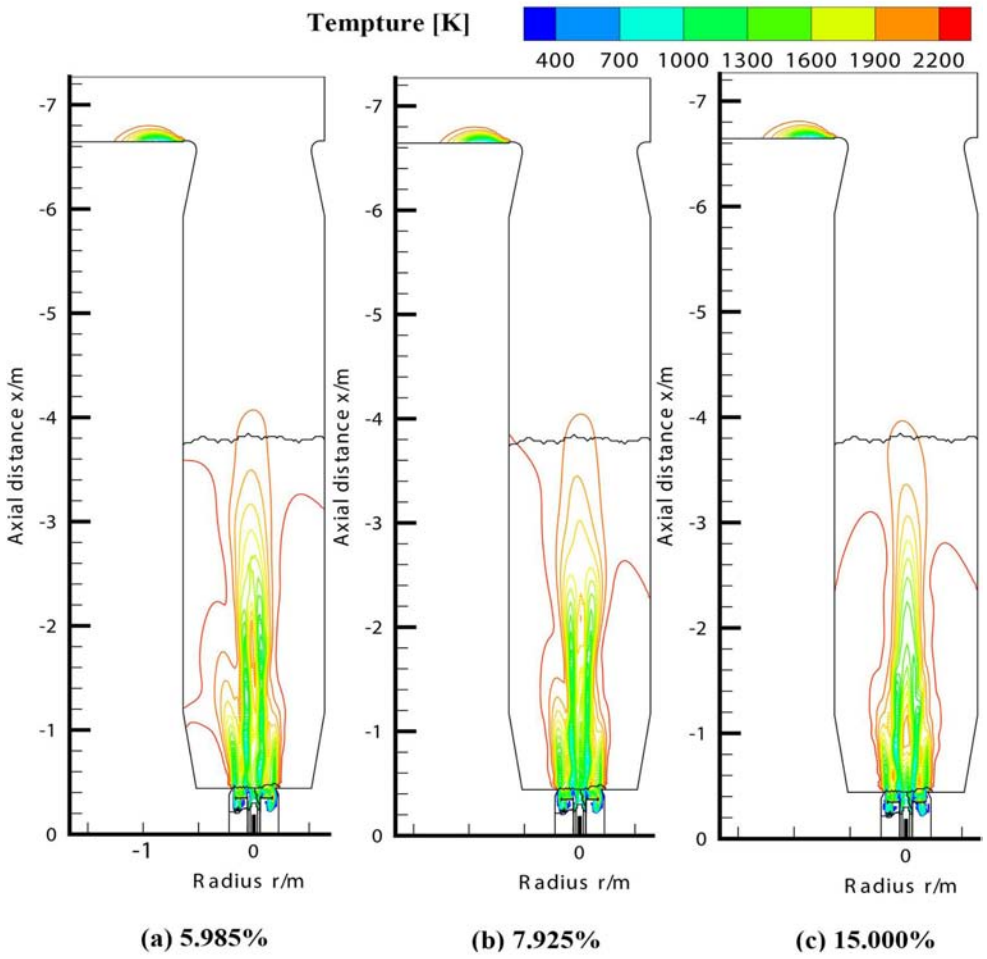

Fig. (6). Temperature distributions at different primary to secondary air ratios.

primary to secondary air ratios affect the combustion reaction by changing the oxygen content and velocity distribution of gas. Thereby the shape of the flames can be controlled.

3.4. Distributions of the CO Concentration

As intermediate products CO is produced during the combustion process, the rule of how combustion reaction is

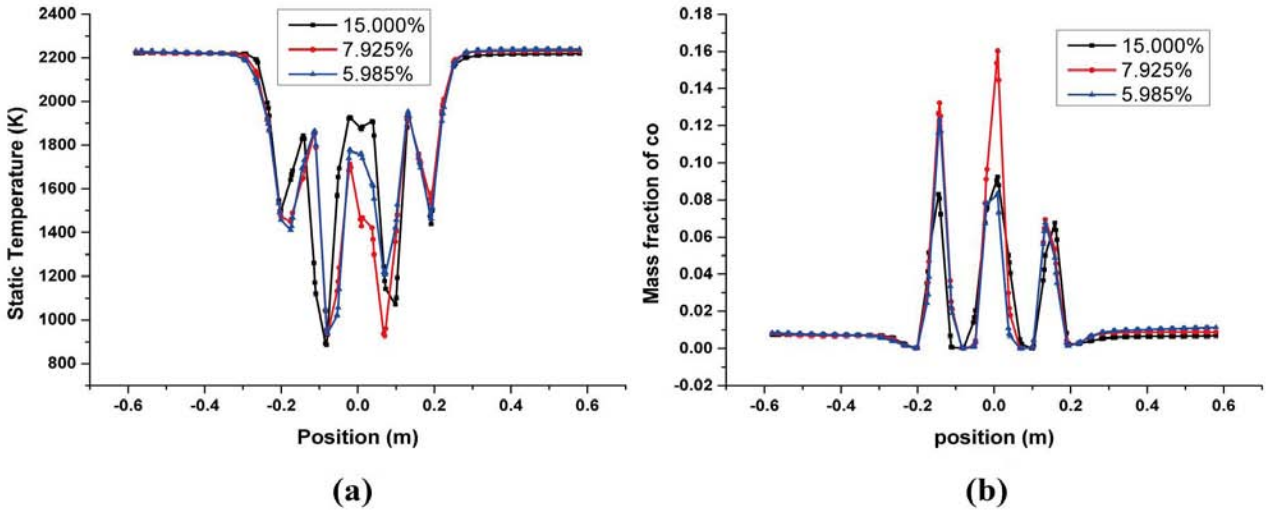

Fig. (7). Variations of temperature and CO mass fractions along line **A-B** shown in Fig. (**5b**) at different primary to secondary air ratios.

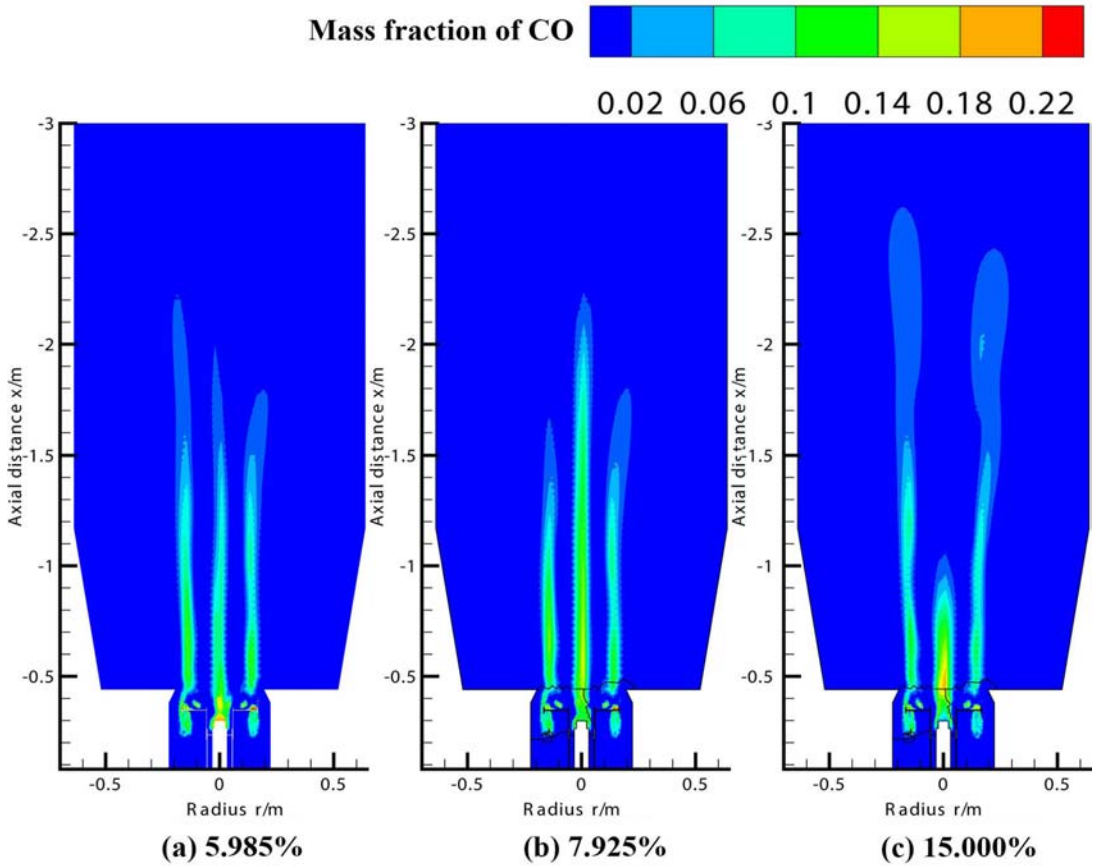

Fig. (8). Mass fraction distributions of CO at different primary to secondary air ratios.

affected by different primary to secondary air ratios is analyzed through observing the distributions of the intermediate products CO. The CO mass fraction distributions inside the boiler furnace under conditions of different primary to secondary air ratios are shown in Fig. (**8**). With the amount of wind increasing, the length of the CO mass fraction distribution area becomes shorter in the inner flames but longer in the outer flames. This is because there is more primary air ejected from the primary air tube and less secondary air around the outer flames, it accelerates the combustion reaction of gas from center gas tube but slows down the reaction of gas ejected from the annular gas pipe But generally speaking, the combustion efficiency is the highest when the proportion of primary air is 15.000%.

Variations of the CO mass fraction of line A-B under conditions of different primary to secondary air ratios are shown in Fig. (**7b**). Although the oxygen concentration in the central region when the proportion of primary air is 7.925% is higher than that when the proportion is 5.985%, the velocity of primary air is faster, so the gas and air here do not have sufficient time to mixed and the combustion reaction is lower than that when the proportion is 5.985%. The velocity of primary air in the central area when the proportion of primary air is 15.000% is faster, however, the combustion reaction is much faster than that when the proportion is 7.925% because of the higher oxygen concentration.

There comes to a conclusion that the oxygen concentration and the velocity of air flows into the region full of surplus gas are two factors which affect the combustion rate in the area. The high oxygen concentration helps to improve the combustion rate. On the contrary, the excessively fast velocity of excessive air hindered the improvement of the combustion rate. These two factors restrain each other and jointly affect the combustion rate. In this paper, the zone where the combustion reaction is the most drastic is defined as the ideal reaction zone. For premixed gas burner, when the opening degree of secondary air door is relatively small like 15°, the factor of oxygen concentration isn't ideal but the factor of flow velocity is in the ascendant in the central area of line A-B. This causes the faster combustion reaction and an ideal reaction zone more closed to the nozzle of the combustion chamber. While opening degree of secondary air door increases to a certain extent, the oxygen concentration couldn't cooperate with the velocity of air in the ideal state. So that the combustion rate in the central area drops down and the ideal reaction zone is moving away from the combustion chamber nozzle. Continuing to increase the opening degree of secondary air door, the influence of oxygen concentration is greater than that of the airflow velocity, so the combustion rate in this region rises up and the ideal reaction zone becomes closer to the nozzle of the combustion chamber again. Through changing the opening degree of secondary air door, users can adjust the position of the ideal reaction zone to control the flame shape.

3.5. NO_x Emissions

Firstly, the simulation results of the NO_x mass fraction and the generation rates of NO_x and thermal NO_x when the proportion of primary air is 7.925% are analyzed.

According to the relative theoretical analysis [2-10], fuel NO_x can be neglected because there is little organic nitrogen in LNG. Prompt NO_x, also known as transient nitrogen oxides, is formed due to the presence of the carbon-containing radicals in the flames at low temperature when nitrogen fuel is burning. It is generated mainly in the combustion chamber and this formation mechanism of prompt NO_x is not a major source of nitrogen oxide emissions. Therefore, thermal NO_x is generally considered as the main NO_x produced during the liquid natural gas combustion process. Thermal NO_x is formed when nitrogen and oxygen within the combustion gas combine at a relatively high temperature of 1700 K above for a long time. So it is generated inside the boiler furnace. Therefore the simulation of nitrogen oxides emission during the LNG combustion process focuses on the thermal NO_x.

At both ends of the area where the furnace and the burner nozzle are connected, the temperature is high and the velocity of airflow is slower, so there is large amount of thermal NO_x generated here. And the situation at the end of the furnace is formed *via* the accumulation of thermal NO_x generated in the flowing process of the high temperature flue gas. Although generation rates in the middle of the furnace is high, the velocity of the high temperature flue gas is so quick that there is no sufficient time to generate NO_x and the little amount of NO_x generated is also taken part from the high temperature flue gas. So the thermal NO_x concentration is less here.

Distributions of the NO_x generation rate and the thermal NO_x formation rate at different primary to secondary air ratios are shown in Figs. (**11**, **12**), respectively. When the prompt NO_x can be neglected, distributions of the NO_x production rate basically agree well with distributions of the thermal NO_x formation rate in the furnace interior. It also confirmed the inference obtained previously that thermal NO_x is the major nitrogen oxides produced in LNG combustion process.

The NO_x concentration contours at different primary to secondary air ratios along line A-B are shown in Fig. (**10a**). Comparing with the situations in Figs. (**4**, **7**), the result shows that there are lower temperatures, air speeds and

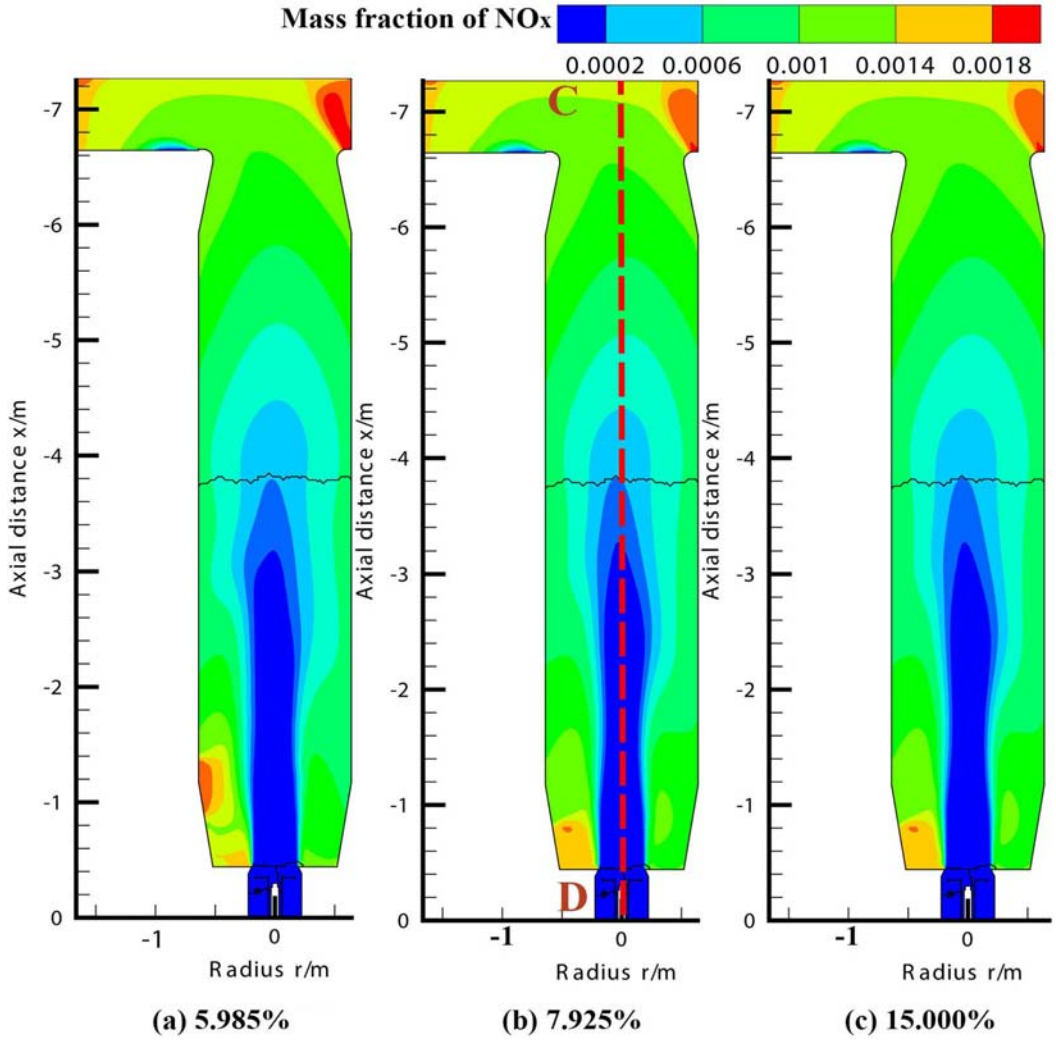

Fig. (9). Mass fraction distributions of NO_x at different primary to secondary air ratios.

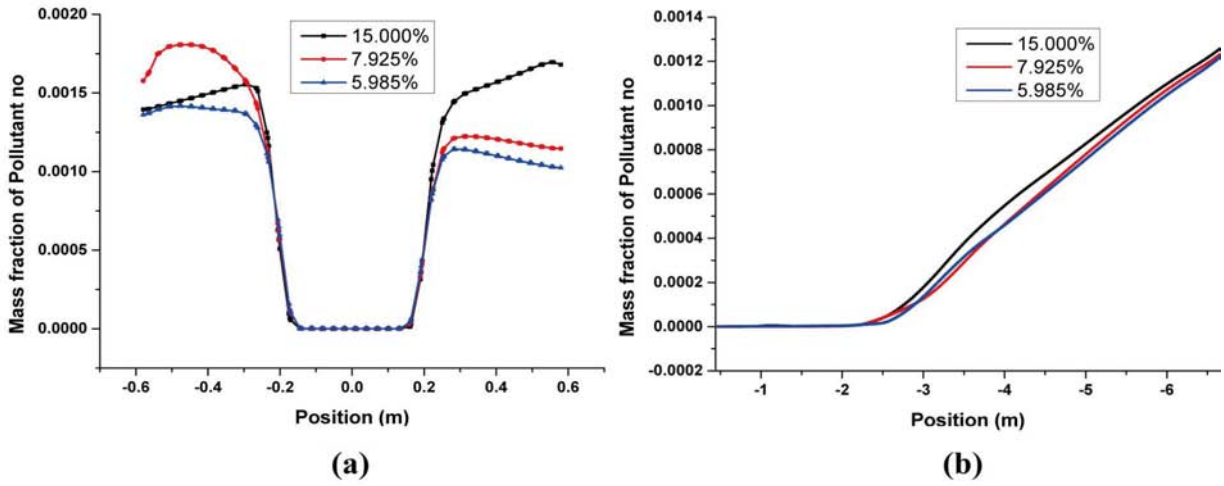

Fig. (10). Variations of NO_x mass fractions along line A-B (a) and line C-D (b).

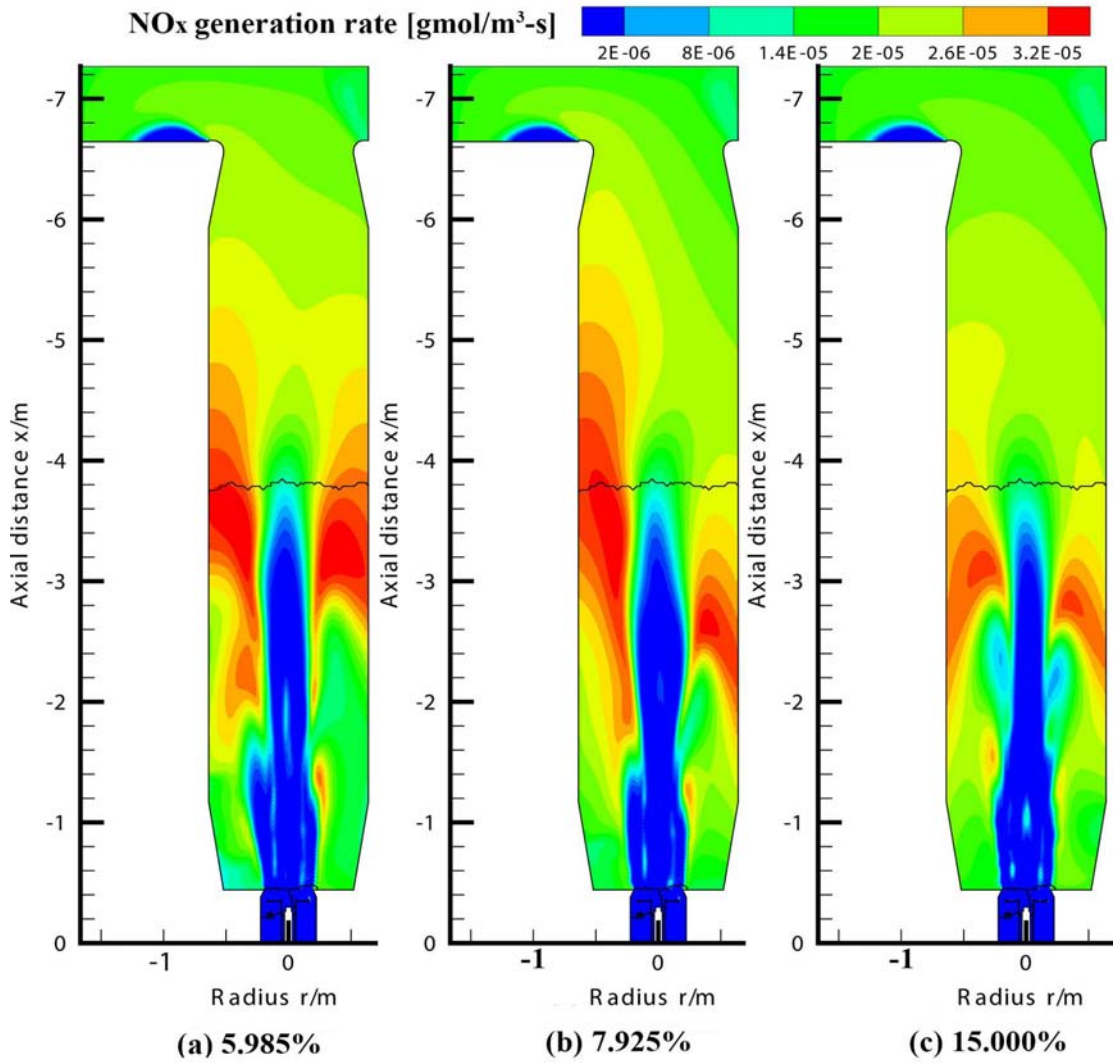

Fig. (11). Generation rate distributions of NO_x at different primary to secondary air ratios.

oxygen concentrations in the internal area of flames, so a small quantity of NO_x is generated here.

Furthermore, this NO_x generated will be taken away by airflow, so the amount of NO_x generated in this area is the

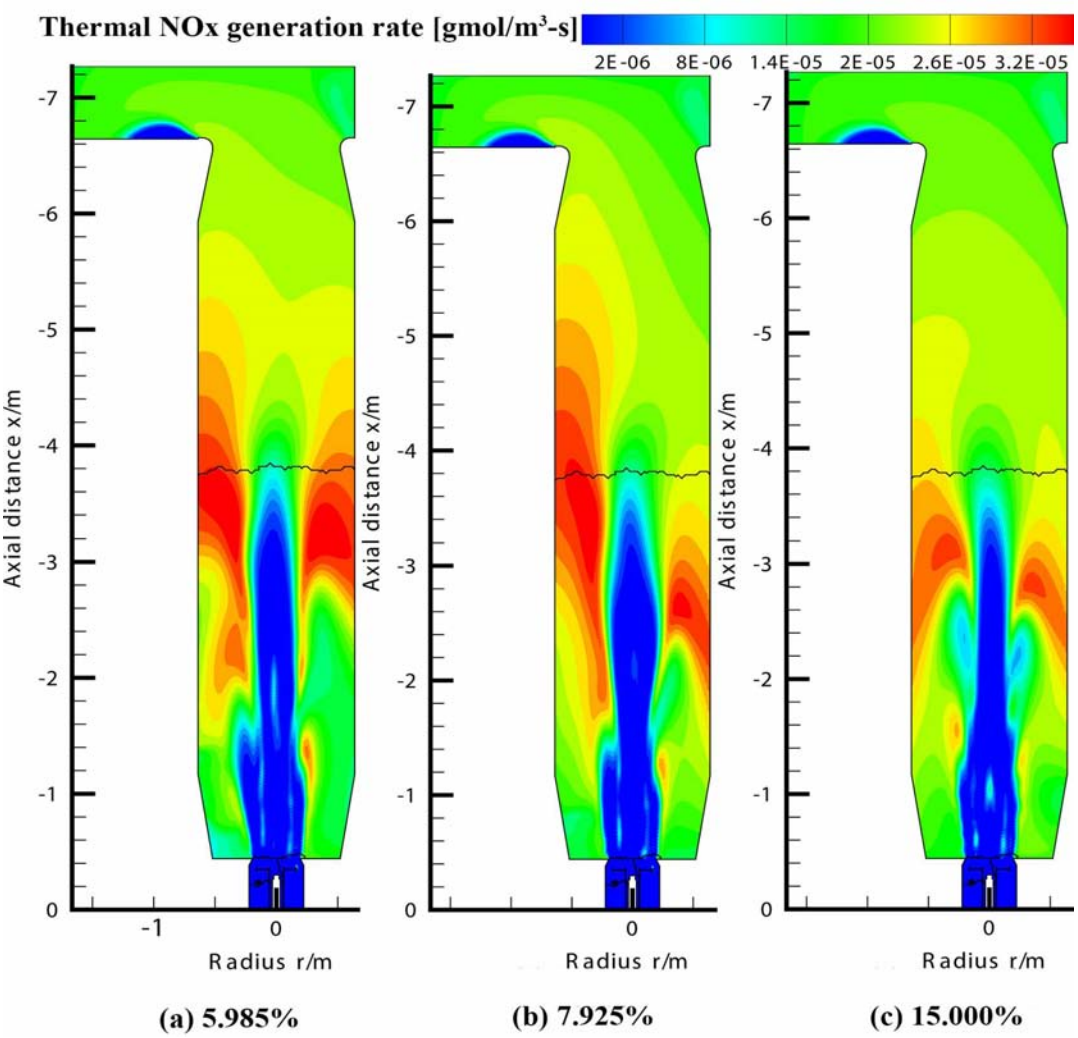

Fig. (12). Generation rate distributions of thermal NO_x at different primary to secondary air ratios.

least at all the three primary to secondary air ratios. When the ratio of primary air is 5.985%, there is more amount of combustion-supporting secondary air outside the flames but less residence time for the high-temperature gas due to the fast velocity, so the minimum mass of NO_x is produced. When the proportion of primary air is 15.000%, the amount of secondary air is the least. But the lowest velocity makes the high-temperature gas can stay for sufficient time. And the two factors at the proportion at 7.925% are moderate, so there are almost the same total amounts of NO_x produced at these two proportions of primary air and just some differences of concentration distributions depending on the distributions of air flow field.

The distributions of NO_x concentration in the center axis line C-D of the furnace are depicted in Fig. (**9b**). The mixed combustion gas near the nozzle of the burner is in the fuel-rich situation, there is no difference of the amounts of NO_x generated at the three proportions of primary air. In the fuel-lean regions, oxygen concentrations have significant influences on the generation of NO_x, so the maximum amount of the NO_x is generated when the proportion of primary air is 15.000%.

Distributions of the NO_x mass fraction at different primary to secondary air ratios are shown in Fig. (**9**). It can conclude that both the total mass fraction and the generation rate of NO_x decrease with the increment of the amount of primary air at both ends of the area where the furnace and the burner nozzle are connected by comparing with the situations in Fig. (**11**). This is because as the amount of primary air increases, the swirling strength of primary air and overall speed of the airflow increases, so residence time for the high temperature flue gas is reduced. Furthermore, oxygen concentration at both ends decreases due to the reduction of the amount of secondary air. These reasons all reduce the generation of NO_x. The distribution situations of the mass fraction and the generation rate of NO_x have a close relationship with the flame shape and the generation rate of thermal NO_x decreases significantly in the regions where the temperature is less than 1700 K.

When the proportion of primary air is 15.000%, the flames are the most concentrated and stable and their heating effect are the best. Meanwhile, the distribution regions of the NO_x generation rate and the mass of NO_x produced are also the smallest. On the contrary, heating efficiency is the worst and the amount of NO_x generated is the largest when the proportion of primary air is 5.985%. Therefore, the most appropriate primary

to secondary air ratio should be chosen through considering comprehensively the situations of heating efficiency and nitrogen oxides emissions which are according to the combustion process of the premixed gas burner.

CONCLUSION

The characteristics of the combustion temperature, flow velocity, CO distribution and NO_x emissions of a 10 MW premixed gas burner in diverse primary to secondary air ratios are numerically investigated using comprehensive models. In order to generate accurate predictions and reduce the amount of calculation, the scheme of simulation process is determined that the airflow fields inside the gas burner are simulated first. According to the analysis results, three groups of representative primary to secondary air ratios are selected for combustion simulation program with a simplified model. Taking into account the distributions of air flow field in the combustion chamber entrance are more uniform, the simplified computational domain used for combustion simulation consists of a combustion chamber of the burner and a supporting boiler furnace.

The analysis results show that flames of the burner are divided into the inner and the outer flames that both have doughnut-shapes. The inner flames are the main flame and there is a swirling flow formed between the inner and the outer flames. With the increase of primary to secondary air ratio, the heating area is more concentrated. Meanwhile, the capacity of the swirling flow to absorb the high temperature flue gas enhances, which improves the stability of flames.

The oxygen concentrations and velocities of air restrain each other and jointly affect the combustion rate. Primary to secondary air ratios affect the combustion reaction by changing the oxygen content and the velocity distributions of gas. Thereby the shape of the flames can be controlled.

Thermal NO_x which generated mainly inside the boiler furnace is generally considered as the main NO_x produced during the liquid natural gas combustion process. Distribution situations of the mass fraction and generation rate of NO_x have a close relationship with the flame shape.

Two indicators of combustion quality are obtained. The first one is the heating effect of the combustion chamber and the second one is the situation of NO_x generation. Analysis shows that the primary to secondary air ratio which has a better heating effect also has a lower NO_x formation rate. Therefore these two evaluation index needs to be comprehensively considered in the practical application and chosen appropriately to achieve the best combustion quality for the gas burner.

CONFLICT OF INTEREST

The authors confirm that this article content has no conflict of interest.

ACKNOWLEDGEMENTS

This work was partially supported by the Innovation Foundation Program (No. 2013J4400223) and Business Incubator Project (No. 2013J4200015) from Technology and Information Bureau of Guangzhou City, China.

REFERENCES

[1] Vié, A.; Jay, S.; Cuenot, B.; Massot, M. Accounting for polydispersion in the eulerian large eddy simulation of the two-phase flow in an aeronautical-type burner. *Flow Turbulence Combust.*, **2013**, *90*, 545-581.

[2] Xue, X.C.; Yu, Y.G.; Zhang, Q. Study on expansion characteristic of twin combustion gas jets in five-stage cylindrical stepped-wall observation chamber. *Flow Turbulence Combust.*, **2013**, *91*, 139-155.

[3] Li, P.F.; Mi, J.C.; Dally Bassam, B. Premixed moderate or intense low-oxygen dilution (MILD) combustion from a single jet burner in a laboratory-scale furnace. *Energ. Fuel.*, **2011**, *25*(7), 2782-2793.

[4] Jing, J.P.; Li, Z.Q.; Zhu, Q.Y. Influence of primary air ratio on flow and combustion characteristics and NOx emissions of a new swirl coal burner. *Energy*, **2011**, *36*(2), 1206-1213.

[5] Cavaliere, D.E.; Kariuki, J.; Mastorakos, E.A. Comparison of the blow-off behaviour of swirl-stabilized premixed, non-premixed and spray flames. *Flow Turbulence Combust.*, **2013**, *91*, 347-372.

[6] Singh, A.; Mann, M.; Kissel, T.; Brübach, J.; Dreizler A. Simultaneous measurements of temperature and Co concentration in stagnation stabilized flames. *Flow Turbulence Combust.*, **2013**, *90*, 723-739.

[7] Trisjono, P.; Kleinheinz, K.; Kang, S.; Pitsch, H. Large eddy simulation of stratified and sheared flames of a premixed turbulent stratified flame burner using a flamelet model with heat loss. *Flow Turbulence Combust.*, **2014**, *92*, 201-235.

[8] Vascellari, M.; Schulze, S.; Nikrityuk, P.; Safronov, D.; Hasse, C. Numerical simulation of pulverized coal MILD combustion using a new heterogeneous combustion sub-model. *Flow Turbulence Combust.*, **2014**, *92*, 319-345.

[9] Choi, C. R.; Kim, C. N. Numerical investigation on the flow, combustion and NOx emission characteristics in a 500 MWe tangentially fired pulverized-coal boiler. *Fuel*, **2009**, *88*, 1720-1731.

[10] Chaney J.; Liu H.; Li J. An overview of CFD modelling of small-scale fixed-bed biomass pellet boilers with preliminary results from a simplified approach. *Energy Convers. Manage.*, **2012**, *63*, 149-156.

[11] Perumal, K.; Krishnan, J. A CFD study of the effect of venturi geometry on high pressure wet gas metering. *Int. J. Oil, Gas Coal Tech.*, **2013**, *5*(6), 549-566.

[12] Park, H.; Faulkner, M.; Turrell, M. Coupled fluid dynamics and whole plant simulation of coal combustion in a tangentially-fired boiler. *Fuel*, **2010**, *89*, 2001-2010.

[13] Fang, Q.; Wang, H.; Wei, Y. Numerical simulations of the slagging characteristics in a down-fired, pulverized-coal boiler furnace. *Fuel Process. Technol.*, **2010**, *91*, 88-96.

[14] Vuthaluru, H. B.; Vuthaluru, R. Control of ash related problems in a large scale tangentially fired boiler using CFD modeling. *Appl. Energ.*, **2010**, *87*, 1418-1426.

[15] Klapdor, E. V.; Mare, F.; Kollmann, W.; Janicka, J.A. Compressible pressure-based solution algorithm for gas turbine combustion chambers using the PDF/FGM model. *Flow Turbulence Combust.*, **2013**, *91*, 209-247.

[16] Yang, Y.B.; Yamauchi H.; Nasserzadeh J.; Swithenbank J. Effects of fuel devolatisation on the combustion of wood chips and incineration of simulated municipal solid wastes in a packed bed. *Fuel*, **2003**, *82*, 2205-2221.

[17] FLUENT 6.3 User's guide.; Fluent Inc., **2006**.

Received: June 11, 2014 Revised: October 23, 2014 Accepted: October 24, 2014